

# Magma source and tectonic setting of the Dunde granite in the Western Tianshan: constraints from geochronology, geochemistry, and Sr–Nd–Hf isotopes

Zhaode Xia<sup>1</sup>  · Haibo Ding<sup>2</sup> · Yanjiao Ru<sup>3</sup>

Received: 7 March 2023 / Revised: 17 May 2023 / Accepted: 23 May 2023 / Published online: 8 June 2023  
© The Author(s), under exclusive licence to Science Press and Institute of Geochemistry, CAS and Springer-Verlag GmbH Germany, part of Springer Nature 2023

**Abstract** The Dunde iron-zinc polymetallic deposit is one of large iron deposits occurred in the Awulale Metallogenic Belt, Western Tianshan (NW-China). This study reports new geochronology and geochemistry for granite in the Dunde mining area in order to constrain the tectonic-magmatic activities and metallogenesis of this region. Granites in the southwest of Dunde mining area are mainly syenogranites intruded into volcanics of the Dahalajunshan Formation in the Early Carboniferous, and they are far from the area where ore bodies and mineralized altered rocks are widely developed. LA-ICP-MS U-Pb zircon dating indicates that Dunde syenogranite was at  $306.8 \pm 1.0$  Ma, which could constrain the upper limit of metallogenic age for this deposit. The Dunde granites are high  $\text{SiO}_2$  (73.41–80.07 wt%), high differentiation index (D.I. = 89.7–95.0), weakly peraluminous to metaluminous ( $\text{A/CNK} = 0.94\text{--}1.08$ ), and they are enriched in LILE and LREE and depleted in Eu, Ba, Sr and  $\text{P}_2\text{O}_5$ , indicating that they belong to highly fractionated I-type granite. Based on  $\varepsilon_{\text{HF}}$  values (+ 9.2 to + 10.5) for zircon and high  $\varepsilon_{\text{Nd}}(t)$  values (+ 4.7 to + 5.8) for whole-rock, and the two-stage model ages for 601–735 Ma, suggest that the magma source could be the juvenile lower crust. Combined with

regional geological setting, the 306.8 Ma Dunde granites are formed in post-collision extensional tectonic setting.

**Keywords** Granite · Geochemistry · Magma source · Tectonic setting · Dunde deposit · Western Tianshan

## 1 Introduction

Granite is an important part of continental crust and a window to understanding the orogenic process and crustal evolution (Amit et al. 2003; Peccerillo et al. 2004). At the same time, acidic magmatic activity can provide heat and metal elements for the formation of ore deposits, which is of great significance for mineralization.

The Awulale Metallogenic Belt (AMB) in the Western Tianshan, a part of the Central Asian Orogenic Belt (CAOB) (Xiao et al. 2004; Gao et al. 1998; Wang et al. 2008; Qian et al. 2009), contains many billion tons iron ore deposits (Wang et al. 2019). These deposits occur mainly in the volcanics of Dahalajunshan Formation. Based on geochronology of volcanics from these deposits, the epoch of mineralization in the AMB is mainly in Early Carboniferous at ca. 330–316 Ma (Feng et al. 2010; Jiang et al. 2014; Zhang et al. 2012) and Late Carboniferous at ca. 310–305 Ma (Jiang et al. 2012). The tectonic setting of the ore-hosting volcanic rocks is disputed between continental rift (Che et al. 1996; Xia et al. 2004) and continental arc setting (Gao et al. 1998, 2009; Wang et al. 2007; Zhu et al. 2009; Jiang et al. 2012, 2014; Zhang et al. 2012). There are different metallogenesis models for these deposits in the AMB, such as VMS deposits, skarn deposits, magmatic and hydrothermal polygenetic deposits, and hydrothermal deposit models (Zhao et al. 2006; Feng

✉ Zhaode Xia  
karlde@163.com

<sup>1</sup> School of Earth Science and Resources, Chang'an University, Xi'an 710054, Shaanxi, China

<sup>2</sup> The Third Geological Branch, Xinjiang Geological and Mineral Bureau, Kuerle, Xinjiang 841000, China

<sup>3</sup> Geophysical and Geochemical Exploration Corporation, Bureau of Geological Exploration for Nonferrous Metals in Northwest China, Xi'an 710068, Shaanxi, China

et al. 2010; Wang et al. 2011, 2019; Hong et al. 2012; Jiang et al. 2014; Duan et al. 2014; Ge et al. 2014; Yan et al. 2020; Li et al. 2020). Different from other deposits, the Dunde deposit is the unique large iron deposit with symbiotic zinc and associated gold in the AMB. Although the Dunde deposit has been extensively studied in terms of petrology, geochemistry, chronology, and mineralization (Duan et al. 2014; Jing 2016; Ding 2017; Ge et al. 2014; Yan et al. 2018, 2020; Li et al. 2020), the tectonic setting and mineralization are still controversially. It's still debatable whether this deposit belongs to skarn-type deposits, and the study of intrusive rocks in the mining area is helpful to better understand the problem. Furthermore, the study of intrusive rocks in this Dunde iron deposit area is relatively weak, so the nature of the source area deserves further study. In this study, we present geochronology, geochemistry, and Nd-Hf isotopic data from the granite in the Dunde mining area of the AMB. We further intend to constrain the genesis of the granite through comprehensive research and define the formation of the Dunde deposit.

## 2 Geological setting

There are many important large-scale iron ore deposits in the AMB (Fig. 1) such as Beizhan, Dunde, Zhibo, Chagangnuoer, Songhu and other deposits. In these mining areas, the strata are mainly Silurian to Jurassic rocks (Gao et al. 1998; Li et al. 2009; Feng et al. 2010; Hu et al. 2000; Li et al. 2009; Wang et al. 2014a, b). The Silurian strata consist of flysch, carbonate and volcanic formation. The Upper Devonian is a set of littoral—marine alternating volcanic-normal clastic rock and carbonate formation, while the Middle Devonian is a set of shallow marine volcanic-clastic rock with a small amount of normal clastic rock. The Carboniferous strata is the most widely distributed strata in this area. The Dahalajunshan formation of Lower Carboniferous is composed of marine volcanic eruption-sedimentary clastic rocks intercalated with carbonate rocks. The first subgroup of the Dahalajunshan formation consist of gray-green dacite tuffaceous breccia, andesitic crystalline tuff, tuffaceous conglomerate, limestone, andesite, diabase porphyrite. The second sub-group of the Dahalajunshan formation is gray to grey-green rhyolite fused tuff, white and gray giant thickness bedded crystalline limestone, and crystal-lithic tuff. The third subgroup is mainly gray-green andesitic crystal clastic vitric tuff intercalated with diorite porphyrite and andesitic porphyrite. The Yishilik Formation of Upper Carboniferous is mainly a set of volcanic breccia, tuff and lava, partially interlaced with normal sedimentary rocks and limestones, and has a flysk-like formation with continental and marine interaction. Permian is a yellowish-gray—gray normal

terrigenous clastic molasse formation (Feng et al. 2010; Allen et al. 1992).

The Dunde deposit is controlled by volcanic mechanisms and occurs in the volcanics of Dahalajunshan Formation. The host rocks are mainly basaltic tuff, dacitic crystalline tuff, dacite and andesite (Fig. 2). A total of 45 iron-zinc and zinc ore bodies have been delineated in the latest exploration results, the main Fe I ore body is estimated to contain 139Mt iron, 1.29Mt zinc and 28.91 tons of associated gold (Ding et al. 2017). The intrusive rocks exposed in the Dunde mining area mainly are granite and diorite. The zircon U-Pb ages for these in the deposits are as follows: 295.8 Ma and 305.3 Ma for syenogranite and 301 Ma for diabase dykes (Duan et al. 2014; Kang 2018).

## 3 Petrography of granite intrusions

Abundant granite intrusions mainly distributed in the southwest of the Dunde deposits and intruded the volcanics of the Dahalajunshan Formation, Early Carboniferous (Figs. 2, 3a). They are not contacted with limestone and far from the area where ore bodies and mineralized altered rocks are widely developed (Fig. 2). The main rock types of granite are syenogranite, fleshy red, medium—coarse granular texture and graphic texture (Fig. 3b). The rocks mainly consist of orthoclase (55–60 %), quartz (30–40 %), plagioclase (5–10 %) and biotite (< 5 %). Plagioclase is grayish white, self-shaped—semi-self-shaped plate columnar, 2–6 mm and some grains have been altered to sericite (Fig. 3f); Orthoclase is mainly semi-automorphic to other-shape and particle size of 2–6 mm, and most grains have been altered to kaolinite (Fig. 3e). Quartz is packed in other shapes between the minerals, and some quartz and orthoclase symbiosis constitute graphic-like texture (Fig. 3c–d). Biotite is distributed in self-shaped to semi-self-shaped columnar and lamellar forms, and most biotite grains have been altered to chlorite and magnetite (Fig. 3e–f).

## 4 Analytical methods

Zircon U-Pb dating and hafnium isotope were performed using the RESOlution LR 193 nm laser denudation system manufactured by Australian Scientific Instruments at LA-MC-ICP-MS at Nanjing FocuMS Technology Co. Ltd. The 193 nm ArF excimer laser, homogenized by a set of beam delivery systems, was focused on zircon surface with a fluence of 3.5 J/cm<sup>2</sup>. The ablation protocol employed a spot diameter of 50 μm at an 8 Hz repetition rate for 40 s (equating to 320 pulses). Helium was applied as a carrier gas to efficiently transport aerosol to MC-ICP-MS.

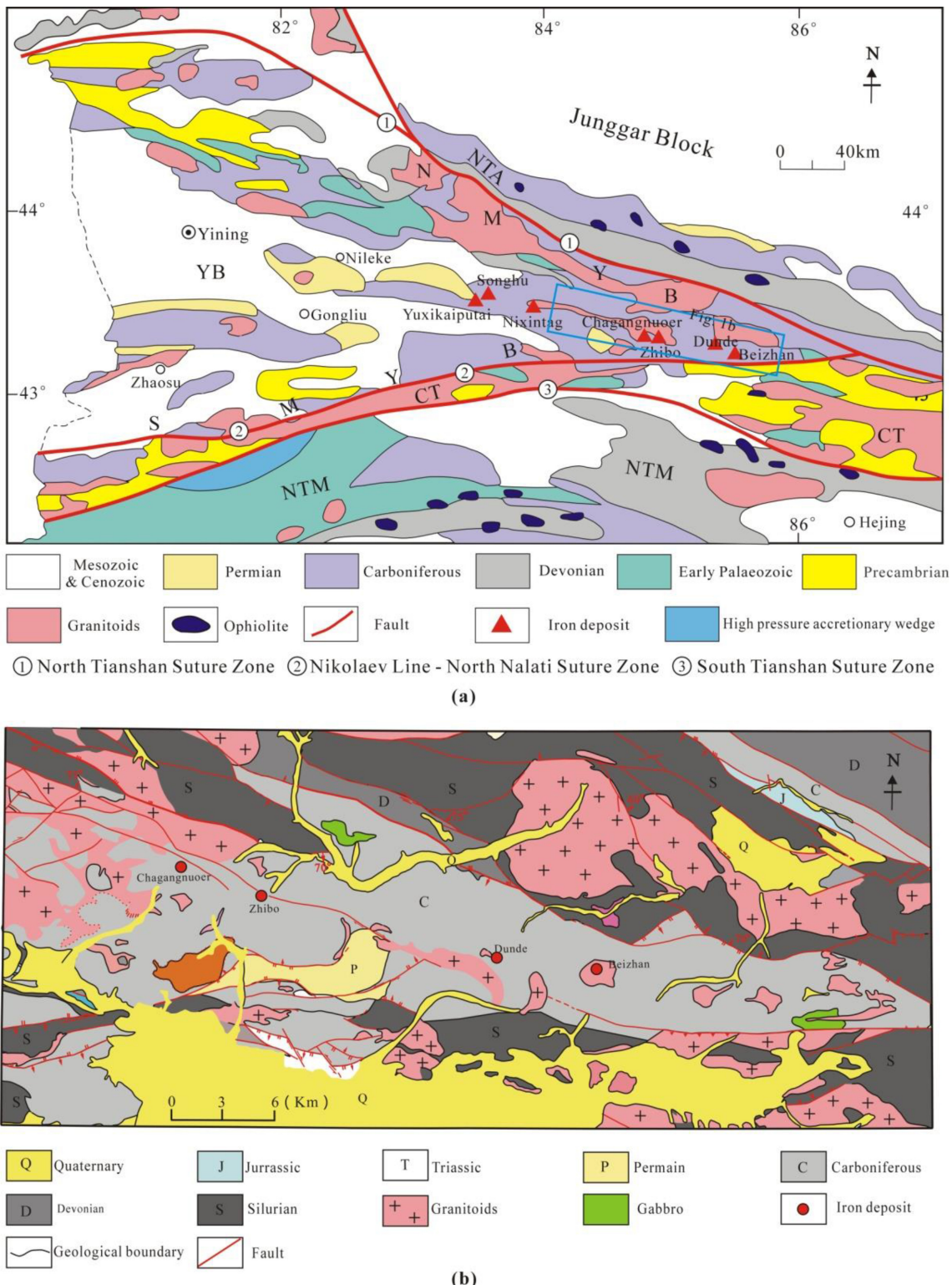


**Fig. 1** **a** Simplified geological map of West Tianshan Mountains (modified after Gao et al. 2009). **b** Geological map of the Chagangnuoer–Beizhan Iron deposits (modified after Wang et al. 2019)



**Fig. 2** Simplified geological map of the Dunde Iron deposits (modified after Duan et al. 2014; Jing 2016)

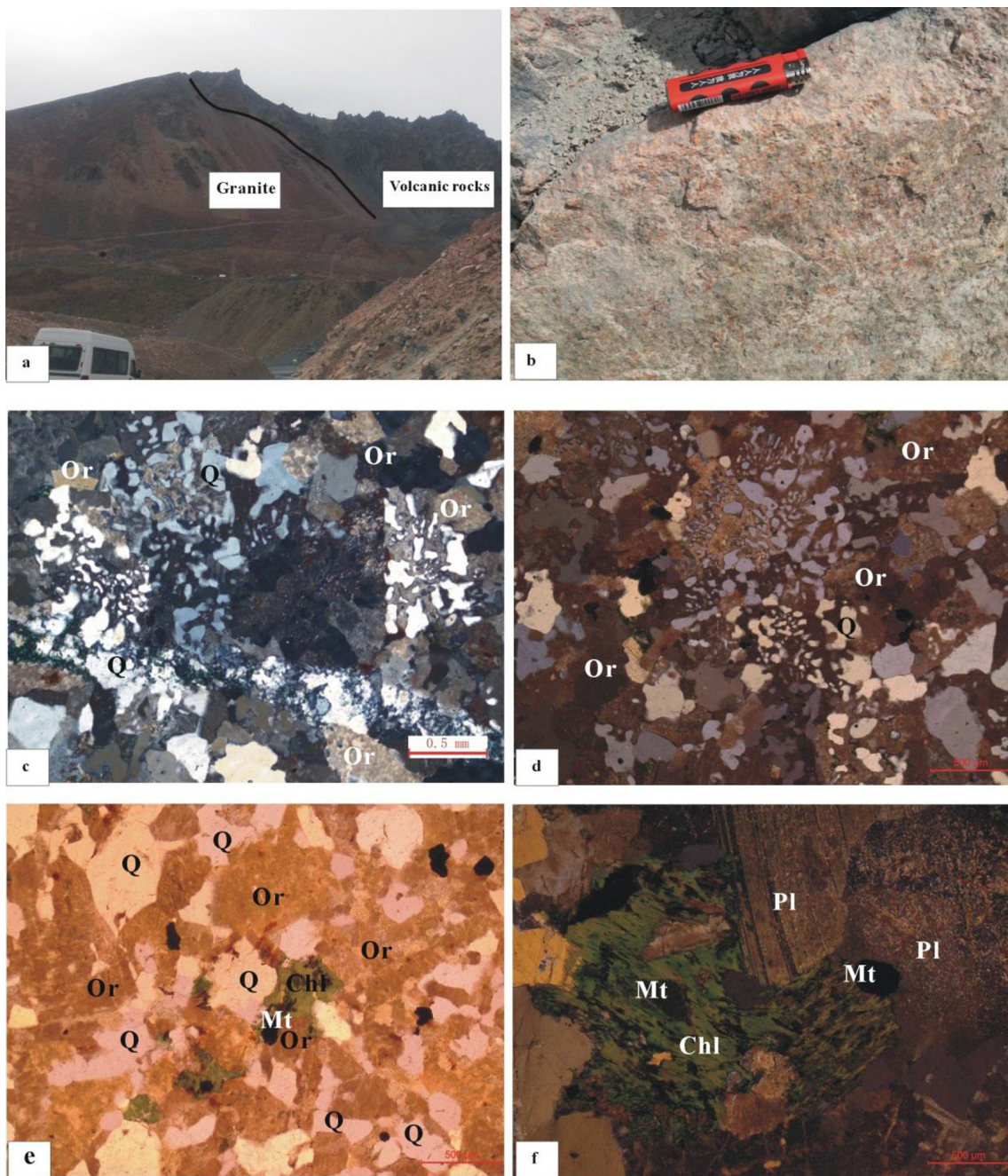


**Fig. 3** Field photos and representative photomicrographs for the Dunde granites in the Western Tianshan. **a** Granitoid intrusions intruded the volcanic host rocks of the iron mineralization in the Early Carboniferous Dahalajunshan Formation. **b** The Dunde granites mainly consist of quartz (Q) and orthoclase(Or). **c, d**, Quartz and orthoclase (Or) symbiosis constitute graphic-like texture. **e** Orthoclase is altered to kaolinite and biotite (Mt) is altered to chlorite and magnetite. **f** Plagioclase (Pl) is altered to sericite and biotite (Mt) is altered to chlorite (Chl) and magnetite (Mt)

Standard zircons (including GJ-1, 91500, Plešovice, Mud Tank, Penglai) were treated as quality control for every five unknown samples. The analytical procedures of the LA-MC-ICP-MS analytical system for zircon U-Pb dating and hafnium isotope are described in detail by Jackson et al. (2004) and Geng et al. (2017), respectively, and the zircon

U/Pb data and Hf isotope data are presented in Tables 1 and 2, respectively.

The whole-rock major oxides were measured by a PANalytical Axios mAX X-ray fluorescence (XRF) spectrometry, while the trace elements were analyzed with an Agilent Technologies 7700  $\times$  quadrupole ICPMS at Nanjing FocuMS Technology Co. Ltd. The analytical

**Table 1** Zircon LA-ICP-MS U–Pb isotopic data of sample H-1 from the Dunde granites

Analysis No	Th ppm	U ppm	$Pb_c$ ppm	$^{232}\text{Th}/^{238}\text{U}$	Ratios						Ages			
					$^{207}\text{Pb}/^{206}\text{Pb}$		$^{207}\text{Pb}/^{235}\text{U}$		$^{206}\text{Pb}/^{238}\text{U}$		$^{207}\text{Pb}/^{235}\text{U}$	$^{206}\text{Pb}/^{238}\text{U}$		
					Ratio	$1\sigma$	Ratio	$1\sigma$	Ratio	$1\sigma$	Age (Ma)	$1\sigma$	Age (Ma)	$1\sigma$
DDH-1-15	1599	2250	0	0.710535	0.053154	0.000585	0.355807	0.00411	0.048373	0.000304	309.1	3	304.5	2
DDH-1-14	937.1	1493	0.258	0.627453	0.051662	0.000649	0.346348	0.004492	0.048466	0.000328	302	3	305.1	2
DDH-1-19	1213	2022	0.703	0.599788	0.052148	0.000576	0.350273	0.004127	0.048642	0.000334	304.9	3	306.2	2
DDH-1-08	2395	3559	0	0.673011	0.052513	0.000529	0.353493	0.003944	0.048663	0.000353	307.3	3	306.3	2
DDH-1-12	1808	2759	0.07	0.655316	0.053014	0.000596	0.358092	0.004381	0.048762	0.000349	310.8	3	306.9	2
DDH-1-16	1880	2848	0.94	0.660152	0.053465	0.000564	0.36128	0.003878	0.048926	0.000329	313.2	3	307.9	2
DDH-1-02	1676	2254	0.115	0.74366	0.052846	0.000597	0.358119	0.004392	0.048957	0.000319	310.8	3	308.1	2
DDH-1-03	3277	5162	1.128	0.634856	0.05297	0.000533	0.359089	0.003963	0.048972	0.000316	311.5	3	308.2	2
DDH-1-21	2587	6332	2.052	0.408591	0.054413	0.0009	0.361669	0.00643	0.047982	0.000665	313.5	5	302.1	4
DDH-1-29	1069	1514	1.321	0.706137	0.053897	0.001051	0.362694	0.007938	0.04832	0.000573	314.2	6	304.2	4
DDH-1-27	2471	4804	1.352	0.514427	0.054802	0.000912	0.368635	0.00677	0.048396	0.000545	318.6	5	304.7	3
DDH-1-22	1232	3461	0.684	0.355926	0.05465	0.000905	0.372811	0.00665	0.049159	0.000501	321.7	5	309.4	3
DDH-1-30	69.06	122.7	1.173	0.562559	0.053117	0.002609	0.344452	0.01053	0.047972	0.000778	300.5	7	302.1	5

**Table 2** Zircon Lu–Hf isotopic data of the granites from the Dunde iron deposit

Sample	Age(Ma)	$^{176}\text{Lu}/^{177}\text{Hf}$	$^{176}\text{Hf}/^{177}\text{Hf}$	2 s	$(^{176}\text{Hf}/^{177}\text{Hf})_i$	$\varepsilon_{\text{Hf}}(t)$	$T_{\text{DM}}$ (Ma)	$T_{2\text{DM}}$ (Ma)	$f_{\text{Lu/Hf}}$
H-1-02	308.1	0.003719	0.282862	0.000009	0.282840	9.19	596.7	735.2	– 0.89
H-1-03	308.2	0.00337	0.282885	0.000008	0.282866	10.1	554.7	676.9	– 0.9
H-1-08	306.3	0.003454	0.282874	0.000008	0.282854	9.64	573.5	704.9	– 0.9
H-1-12	306.9	0.002947	0.282863	0.000009	0.282846	9.37	581.7	722.6	– 0.91
H-1-14	305.1	0.002845	0.282907	0.000009	0.282891	10.93	513.6	621.6	– 0.91
H-1-15	304.5	0.002866	0.282877	0.000006	0.282826	9.82	560.1	692.1	– 0.91
H-1-16	307.9	0.003377	0.282869	0.000007	0.28285	9.52	579.5	713.9	– 0.9
H-1-19	306.2	0.002705	0.282891	0.000006	0.282876	10.41	535.6	655.7	– 0.92
H-1-21	302.1	0.000985	0.282883	0.000007	0.282877	10.37	523	654.8	– 0.97
H-1-22	309.4	0.002357	0.282887	0.000008	0.282873	10.38	537.3	660.1	– 0.93
H-1-27	304.7	0.002946	0.282875	0.000007	0.282858	9.73	564.3	697.6	– 0.91
H-1-29	304.2	0.003145	0.282892	0.000007	0.282874	10.29	541.9	661.9	– 0.91
H-1-30	302.1	0.000773	0.282891	0.000009	0.282887	10.71	508.2	633.1	– 0.98

**Table 3** Major and trace elements of the granites from the Dunde iron deposit

Sample	DDH1	DDH3	DDH4	DDH5	DDH6	DDH7	DDH8	DDH12
SiO <sub>2</sub>	77.16	74.57	77.21	77.72	80.07	73.41	74.21	75.7
TiO <sub>2</sub>	0.13	0.27	0.15	0.13	0.19	0.25	0.23	0.27
Al <sub>2</sub> O <sub>3</sub>	11.65	12.48	12	11.89	10.29	13.35	12.73	12.27
Fe <sub>2</sub> O <sub>3</sub> <sup>T</sup>	0.59	1.74	1.32	0.8	1.27	1.27	1.88	0.98
MnO	0.02	0.04	0.02	0.02	0.02	0.04	0.03	0.02
MgO	0.1	0.22	0.15	0.1	0.13	0.18	0.21	0.21
CaO	1.55	0.92	0.5	0.61	0.61	1.66	0.8	1.16
Na <sub>2</sub> O	2.79	2.69	2.84	2.88	2.21	3.11	3.08	3.11
K <sub>2</sub> O	4.6	5.19	5.23	4.85	4.42	4.87	5.41	4.94
P <sub>2</sub> O <sub>5</sub>	0.01	0.04	0.01	0.01	0.01	0.04	0.03	0.04
LOI	1.5	1.4	0.65	0.87	0.86	2.12	0.79	1.36
Sum	100.09	99.55	100.08	99.88	100.09	100.3	99.39	100.06
Li	0.5	1.55	0.29	0.92	1.6	0.32	2.41	0.49
Be	2.5	2.84	4.24	2.78	2.14	2.37	4.19	2.79
Sc	2.39	4.22	2.22	2.81	3.28	3.85	4.41	3.33
Ti	757	1550	893	751	1130	1453	1419	1572
V	0.63	6.14	1.11	0.67	2.38	7.91	5.6	6.51
Cr	9.3	11.12	8.93	7.35	21.4	7.24	8.3	11.33
Mn	174	338	181	165	171	332	237	194
Co	0.27	2.63	0.81	0.51	0.72	1.48	1.18	0.33
Ni	1.2	1.97	1.21	0.01	8.76	0.03	0.92	2.43
Cu	0.82	4.33	11.77	3.01	4.85	5.6	6.8	1.2
Zn	11.8	32	18.88	16	17.78	20.6	29.3	18.49
Ga	12.36	12.61	16.24	13.82	11.59	14.87	15.97	12.97
As	3.12	14.32	7.52	4.31	3.97	5.87	7.14	4.77
Se	0.71	0.8	1.35	0.82	0.91	1.02	1.07	0.98
Rb	234	242	259	243	198	227	264	213
Sr	25.7	40	41	28.3	36	42	74	50
Y	24.3	31	42	25.2	27.8	40	41	30
Zr	218	304	166	190	246	256	273	236
Nb	13.62	11.82	14.01	19.13	10.84	12.2	13.05	9.87
Mo	1.1	2.94	1.14	1.18	0.85	1.28	1.53	0.5
Cs	2.54	2.3	1.77	1.83	2.72	2.46	2.29	2
Ba	71	191	80	135	141	211	279	209
La	24.4	15.52	41	29.9	19.63	32	31	22.9
Ce	59	38	110	70	55	80	75	51
Pr	6.24	4.26	11.61	6.89	5.22	9.11	8.53	6.16
Nd	22.7	16.69	46	23.6	20.8	36	31	24.4
Sm	4.52	3.78	8.6	4.47	4.51	7.42	6.71	5.81
Eu	0.14	0.42	0.15	0.15	0.21	0.7	0.76	0.8
Gd	3.9	3.96	7.65	4.04	4.3	6.77	6.24	5.36
Tb	0.61	0.73	1.25	0.68	0.74	1.1	1.09	0.87
Dy	3.71	4.94	7.61	4.28	4.65	6.67	6.93	5.38
Ho	0.78	1.08	1.56	0.9	1	1.39	1.46	1.11
Er	2.48	3.31	4.57	2.72	3.04	4.18	4.45	3.28
Tm	0.41	0.53	0.68	0.43	0.48	0.65	0.71	0.51
Yb	2.98	3.61	4.43	2.97	3.22	4.37	4.74	3.45
Lu	0.47	0.54	0.64	0.45	0.48	0.65	0.71	0.5

**Table 3** continued

Sample	DDH1	DDH3	DDH4	DDH5	DDH6	DDH7	DDH8	DDH12
Hf	7.58	8.31	6.22	6.86	7.63	7.34	7.93	6.82
Ta	1.46	1.09	1.26	2.52	1.2	0.99	1.35	0.96
W	1.68	6.24	3.13	5.73	2.08	4.34	4.03	1.9
Pb	4.06	7.08	7.95	4.79	7.17	7.28	9.56	6.09
Th	36	23	49	45	35	28.5	29.8	21.9
U	11.96	4.85	10.64	8.22	5.77	6.05	6.84	5.18

uncertainties for both major and trace elements (including the REE) are generally 1–5 %. The detailed analytical procedures are described by Li et al. (2006), and the analyzed elemental compositions are listed in Table 3.

Sr and Nd isotopic analyses were performed using a Nu Plasma II MC-ICP-MS at the Nanjing FocuMS Technology Co. Ltd., following the analytical procedures in Li et al. (2006). Measured  $^{143}\text{Nd}/^{144}\text{Nd}$  and  $^{87}\text{Sr}/^{86}\text{Sr}$  ratios were normalized to  $^{146}\text{Nd}/^{144}\text{Nd} = 0.7219$  and  $^{86}\text{Sr}/^{88}\text{Sr} = 0.1194$ , respectively. Isotopic results of geochemical reference materials BCR-2 ( $^{87}\text{Sr}/^{86}\text{Sr} = 0.705017 \pm 0.000005$ ;  $^{143}\text{Nd}/^{144}\text{Nd} = 0.512649 \pm 0.000003$ ), STM-2 ( $^{87}\text{Sr}/^{86}\text{Sr} = 0.703704 \pm 0.000005$ ;  $^{143}\text{Nd}/^{144}\text{Nd} = 0.512907 \pm 0.000002$ ), AVG-2 ( $^{143}\text{Nd}/^{144}\text{Nd} = 0.512795 \pm 0.000002$ ), GSR-10 ( $^{87}\text{Sr}/^{86}\text{Sr} = 0.704369 \pm 0.000005$ ;  $^{143}\text{Nd}/^{144}\text{Nd} = 0.512762 \pm 0.000003$ ), GSR-15 ( $^{87}\text{Sr}/^{86}\text{Sr} = 0.719369 \pm 0.000005$ ;  $^{143}\text{Nd}/^{144}\text{Nd} = 0.512897 \pm 0.000003$ ) and RGM-2 ( $^{87}\text{Sr}/^{86}\text{Sr} = 0.704170 \pm 0.000004$ ;  $^{143}\text{Nd}/^{144}\text{Nd} = 0.512796 \pm 0.000003$ ) were within the recommended values (Weis et al. 2006). The analytical results are given in Table 4.

## 5 Results

### 5.1 Geochronology

The zircon U–Pb data for the Dunde granite are in Table 1. Most zircon grains are black to gray with an obscure oscillatory texture in the CL images. These zircon grains are long prismatic morphology and are usually 70–160  $\mu\text{m}$  in length with 30–80  $\mu\text{m}$  in width. The Th/U ratios of zircon are 0.21–0.79 (Table 1), greater than 0.1, indicating these zircons crystallized from magma. All analyzed spots yield a weighted mean  $^{206}\text{Pb}/^{238}\text{U}$  age of  $306.8 \pm 1.0$  Ma (Fig. 4), indicating the crystallization age of the Dunde granite.

### 5.2 Whole-rock geochemistry

All granites from the Dunde deposit area are high in  $\text{SiO}_2$  (73.4–80.1 wt%) and alkalis ( $\text{Na}_2\text{O} + \text{K}_2\text{O} = 6.63\text{--}8.48$  wt%). They have low  $\text{TiO}_2$  (0.13–0.27 wt%),  $\text{Al}_2\text{O}_3$  (10.29–13.35 wt%),  $\text{Fe}_2\text{O}_3^{\text{T}}$  (0.59–1.88 wt%),  $\text{MgO}$  (0.10–0.22 wt%) and  $\text{P}_2\text{O}_5$  (0.01–0.04 wt%) (Table 2). In the  $\text{K}_2\text{O}$  vs.  $\text{SiO}_2$  diagram (Fig. 5a), all samples of the Dunde granites plot in the fields of high K-calc-alkaline rocks. All samples have A/CNK [molar ratio of  $\text{Al}_2\text{O}_3/(\text{CaO} + \text{Na}_2\text{O} + \text{K}_2\text{O})$ ] varying from 0.94 to 1.08, and belong to weakly peraluminous to weakly metaluminous (Zen 1986) (Fig. 5b).

All granites have high Rb (198–264 ppm) and low Sr (26–74 ppm) (Table 2), thus with high Rb/Sr ratios (3.59–9.11). They have relatively high LREE and LILE (Rb, Th, U) concentrations (Table 2). In the diagram of chondrite-normalized REE patterns, these granites are characterized by a moderate enrichment in LREE, flat HREEs and remarkable negative Eu anomalies with  $\delta\text{Eu}$  varying from 0.05 to 0.43 (Fig. 6a). Furthermore, it shows enrichments in LILEs and distinct negative Ba, Sr, P, and Ti anomalies in the primitive mantle normalized spidergrams (Fig. 6b).

### 5.3 Strontium and neodymium isotopes

Five Sr, and Nd isotope analyses were carried out for the Dunde granites (Table 3). These rocks have low Sr concentrations, high Rb/Sr ratios, and variable  $^{87}\text{Sr}/^{86}\text{Sr}$  ratios (0.7201–0.7736), and the initial  $^{87}\text{Sr}/^{86}\text{Sr}$  ratios 0.6585–0.7012 is low. These rocks have  $^{143}\text{Nd}/^{144}\text{Nd}$  ratios (0.512752–0.512768) and  $^{147}\text{Sm}/^{144}\text{Nd}$  ratios (0.1141–0.1432) and show small variations in Nd isotopic compositions with  $\varepsilon\text{Nd(t)}$  values varying from 4.7 to 5.8 and juvenile two stage Nd model ages ( $T_{2\text{DM}} = 601\text{--}687$  Ma).

**Table 4** Whole-rock Rb–Sr and Sm–Nd isotopic data of the granites from the Dunde iron deposit

Sample	Age (Ma)	Rb ppm	Sr ppm	$^{87}\text{Sr}/^{86}\text{Sr}$	$^{87}\text{Rb}/^{86}\text{Sr}$	$(^{87}\text{Sr}/^{86}\text{Sr})_{\text{i}}$	Sm ppm	Nd ppm	$^{143}\text{Nd}/^{144}\text{Nd}$	$^{147}\text{Sm}/^{144}\text{Nd}$	$(^{143}\text{Nd}/^{144}\text{Nd})_{\text{i}}$	$\varepsilon_{\text{Nd(t)}}$	$T_{\text{DM}} (\text{Ma})$	$T_{2\text{DM}} (\text{Ma})$
DDH-1	306.8	234.0	25.69	0.773620	26.52	0.657828	4.52	22.66	0.512752	0.12064	0.512509	5.2	655.7	646.1
DDH-4	306.8	258.7	41.18	0.765792	18.28	0.685982	8.6	45.51	0.512767	0.114147	0.512538	5.76	589.2	600.6
DDH-6	306.8	197.6	36.46	0.762510	15.76	0.693697	4.51	20.8	0.512768	0.131016	0.512505	5.11	707.5	653
DDH-8	306.8	264.4	73.71	0.746468	10.42	0.700994	6.71	31.49	0.512755	0.128722	0.512496	4.95	711.9	666.5
DDH-9	306.8	47.57	25.47	0.720119	5.41	0.695504	1.73	7.28	0.512771	0.143192	0.512483	4.69	823.5	687.5

## 5.4 Zircon Lu–Hf isotopes

Zircon Lu–Hf isotope analyses for the granites are shown in Table 2. Among the concordant zircons, 13 were conducted for in-situ Lu–Hf isotopic analysis,  $^{176}\text{Lu}/^{177}\text{Hf}$  ratio for zircon is 0.000773 to 0.003719 and  $^{176}\text{Hf}/^{177}\text{Hf}$  ratio for zircon is 0.282862 to 0.282907. In terms of the zircon age, the initial  $^{176}\text{Hf}/^{177}\text{Hf}$  ratio is 0.282840 to 0.282891. In terms of the zircon  $\varepsilon_{\text{Hf(t)}}$  value from the sample, the points of this sample exhibit positive values (+ 9.2 to + 10.9, with a mean of + 10.0) (Fig. 7) with the  $T_{\text{DM2}} = 622\text{--}735$  Ma (with a mean of 679 Ma).

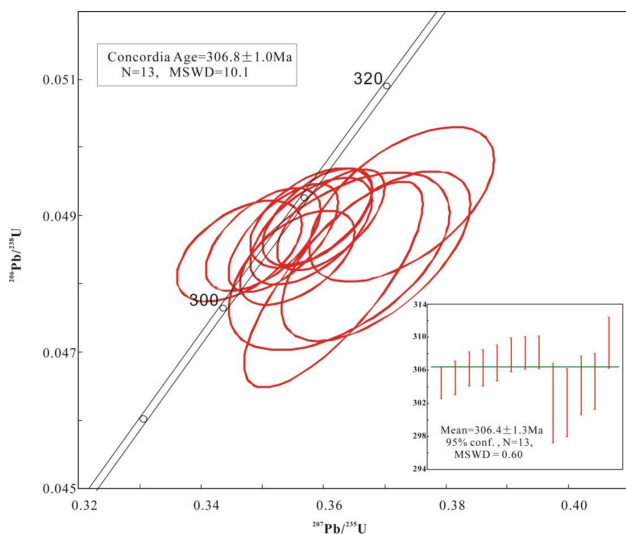
## 6 Discussion

### 6.1 Genesis classification of the Dunde granites

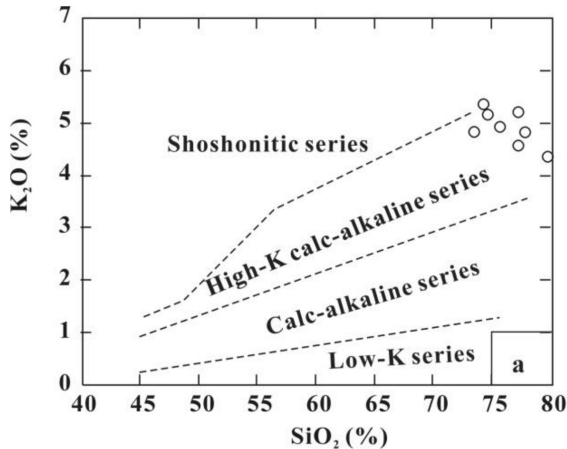
The Dunde granites have A/CNK varying from 0.94 to 1.08 and belong to weakly peraluminous to weakly metaluminous, different from the typical S-type granites with A/CNK > 1.1 (Chappell and White 1974). The Al-enriched minerals have not been observed in the Dunde granites, and the contents of the Corundum-norm for these granites are less than 1%. The  $\text{P}_2\text{O}_5$  contents of these granites are very low (< 0.05%) and decrease with the increase of  $\text{SiO}_2$  (Fig. 7a) (Kong et al. 2018). These observations suggest that the Dunde granites should not be S-type granite.

Meanwhile, there are no alkaline melanocratic minerals such as arfvedsonite, riebeckite, aegirine, and fayalite (Eby 1990, 1992) in the Dunde granites, and they have low  $10,000 \times \text{Ga/Al}$  values (1.03–1.38, average of 1.16) and low Ce values (51–110 ppm) (Fig. 8b), which is distinguishable from A-type granite (Whalen et al. 1987, 2006). In addition, a graphic-like texture is commonly developed in the Dunde granites, which indicates that quartz and feldspar have simultaneous growth in the granites (Fenn 1986). This structure is the product of the rapid crystallization of the melt under the condition of saturated volatiles (Kirkham and Sinclair 1988).

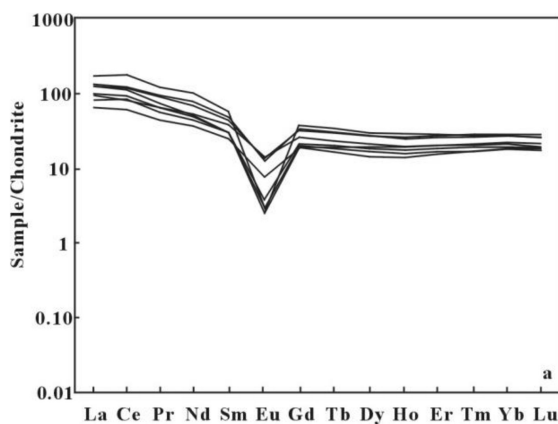
The Dunde granites are characterized by high  $\text{SiO}_2$  (73.41–80.07 wt%, mean of 76.26 wt.%), high  $\text{Na}_2\text{O} + \text{K}_2\text{O}$  (6.63–8.48 wt.%), high differentiation index (D.I. = 89.7–95.0, mean of 93.0), and significant negative Eu anomalies and strong depletion of Nb, Sr, P and Ti, similar to those of highly fractionated granites (Clarkede 1981; Wang et al. 2014a, b). Therefore, these data confirm that the Dunde granites are highly fractionated I-type granite (Fig. 8a–f). The negative anomalies of Eu and Sr are mainly constrained by the fractional crystallization of plagioclase, and depletion of Ba concentration is mainly



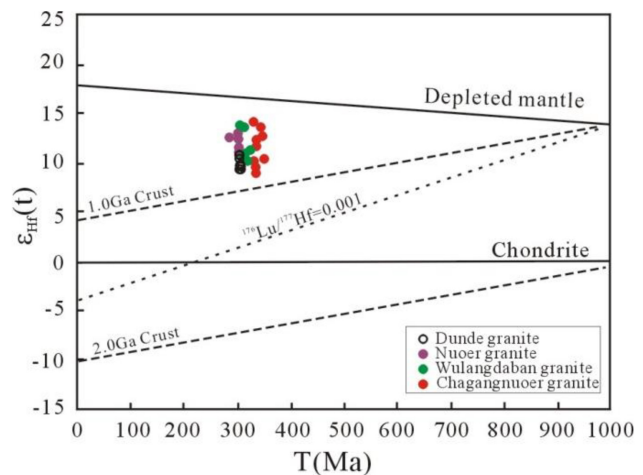
**Fig. 4** LA-ICP-MS U-Pb zircon concordia diagrams for granitoids associated with the Dunde iron deposits



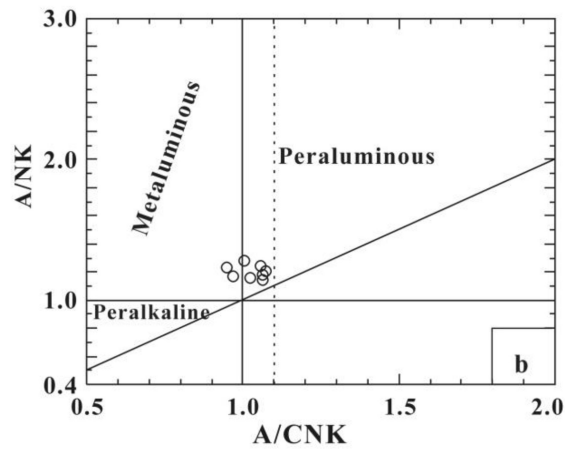
**Fig. 5** Major element diagram for the Dunde granites. **a**  $K_2O$  versus  $SiO_2$  diagram (after Gill 1981) and **b** ACNK versus ACNK diagram (after Maniar and Piccoli 1989)



**Fig. 6** Chondrite-normalized rare earth element diagrams (**a**) and primitive mantle-normalized trace element diagrams (**b**) of granite from the Dunde iron ore deposit. Normalized values are after Sun and McDonough (1989)



**Fig. 7** Zircon U-Pb ages versus  $\epsilon_{Hf}(t)$  values for zircons from the Dunde granite (data for Chagangnuor, Wulangdaban, and Nuor granite are from Li et al. 2006)



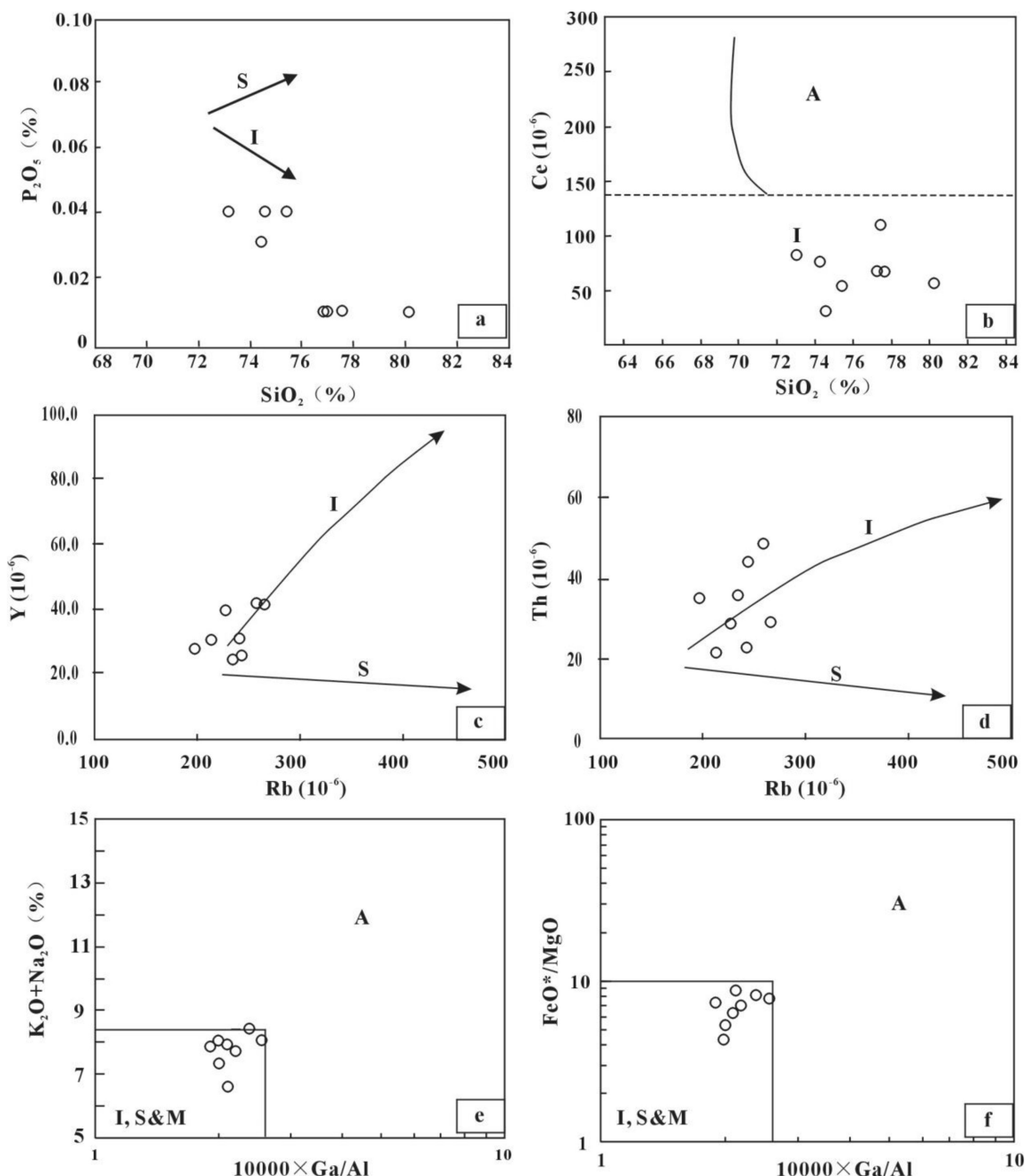


**Fig. 8** Diagram of rock type discrimination for the Dunde granites. Plot of  $\text{SiO}_2$  versus  $\text{P}_2\text{O}_5$  (a) and  $\text{Ce}$  (b);  $\text{Rb}$  versus  $\text{Y}$  (c) and  $\text{Th}$  (d);  $10,000 \times \text{Ga}/\text{Al}$  versus  $\text{Na}_2\text{O} + \text{K}_2\text{O}$  (e) and  $\text{FeO}^*/\text{MgO}$  (f) of the Dunde granites (after Whalen et al. 1987)

constrained by orthoclase (Fig. 9). The variation of La and  $(\text{La}/\text{Yb})_{\text{N}}$  is restricted by apatite.

## 6.2 Petrogenesis of the Dunde granites

The Carboniferous rocks in the Awulale area are mainly intermediate-acid intrusive rocks and volcanic rocks

(Wang et al. 2019), and there are not a large scale of basaltic rocks. Therefore, these granites in the Awulale Metallogenic Belt (AMB) could not be differentiated from limited basaltic magma (Wyllie et al. 1984), and they should be formed by partial melting of crustal materials.

The 306.8 Ma Dunde syenogranite is highly fractionated I-type granite. Whole-rock Nd isotopic and zircon Hf

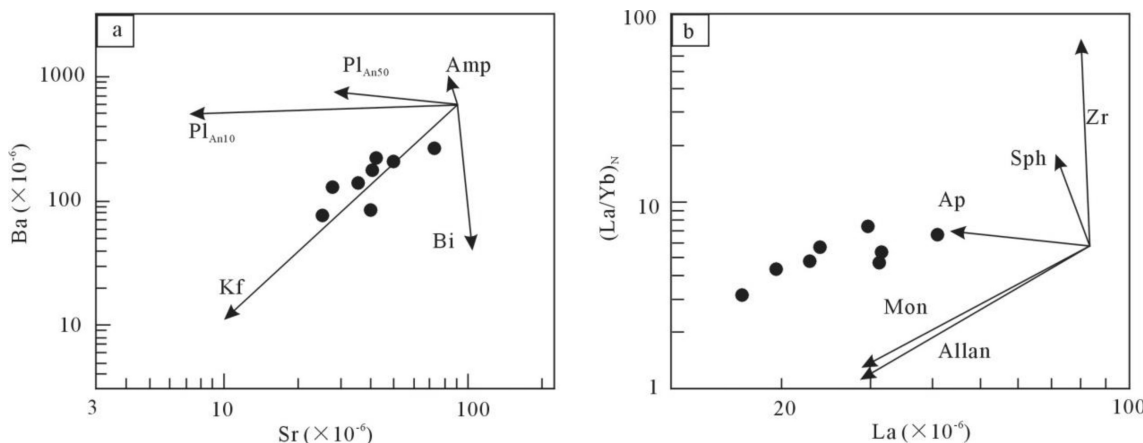


**Fig. 9** Sr–Ba (a) and La–(La/Yb)<sub>N</sub> (b) diagrams showing the fractional crystallization trends for the Dunde granites. Partition coefficients of Sr and Ba are from Blundy and Shimizu (1991) for plagioclase, and from Ewart and Griffin (1994) for other minerals. The fractionation trends for accessory minerals are from Wu et al. (2003). Pl<sub>An10</sub>-plagioclase with An = 10; Pl<sub>An50</sub>-plagioclase with An = 50; Kf-K-feldspar; Bi-biotite; Amp-amphibole; Zr-zircon; Sph-sphene; Apapatite; Mon-monazite; Allan-allanite

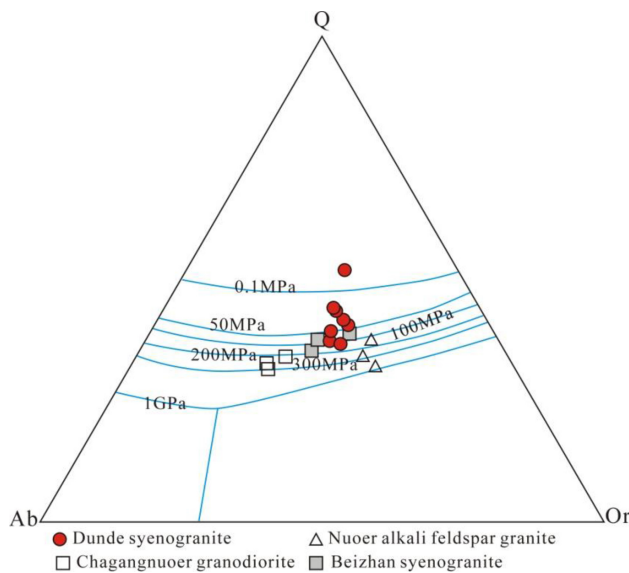


**Fig. 10** Q-Ab-Or diagram for the granites (after Huang and Wyllie 1975)

isotopic compositions of the granites are relatively uniform with  $\varepsilon_{\text{Nd}}(t)$  values varying from 4.7 to 5.8 and  $\varepsilon_{\text{Hf}}(t)$  values ranging from + 9.2 to + 10.9. According to the crustal Nd-Hf isotope correlation array (Vervoort and Blichert 1999), the Hf isotopic compositions of this granite are coupled with the Nd isotopic compositions. Therefore, these isotopic compositions indicate that the magma source of granites may be a depleted mantle nature or a juvenile lower crust. While, the average Ce/Pb and Nb/Ta ratios of the Dunde granites were 10.37 and 10.02, respectively, which was close to that of crustal values (Ce/Pb < 15, Furman et al. 2004; Nb/Ta = 12–13, Barth et al. 2000), far from that of mantle-derived magma value (Ce/Pb = 25 ± 5, Furman et al. 2004; Nb/Ta = 17.5 ± 2.0, Green 1995),

indicating that the magma source of granites should be mainly juvenile crustal material. The Nd and Hf model ages ( $T_{2\text{DM}}$ ) are 601–687 Ma and 622–735 Ma, respectively, which indicates that the differentiation for crustal and mantle can be traced back to Neoproterozoic. These characteristics indicate that the magma source of granites in the Dunde mining area could be the juvenile lower crust rather than the ancient crust.

According to the markedly negative Sr, Ba, and Eu anomalies in the Dunde syenogranite, it is speculated that the source area has a residual Ca-rich plagioclase phase, indicating that the granite has a relatively low diagenetic pressure (less than 0.8 or 1.0 GPa). The normative quartz-albite-orthoclase (Q-Ab-Or) pseudo-ternary (Tuttle and Bowen 1958; Gualda and Ghiorso 2013), which is used to estimate the equilibration pressure for granitic systems, indicates an equilibration pressure of approximately 50–200 MPa for the Dunde syenogranite, similarly with Beizhan syenogranite, while lower than Chagangruoer granodiorite and Nuuo alkali feldspar granite (Fig. 10). Thus, the Dunde syenogranite must be emplaced at shallower levels of the juvenile lower crust.

### 6.3 Tectonic setting and mineralogenetic epoch for the Dunde iron deposit

The geochronology and geochemistry studies of Carboniferous volcanic rocks in the Western Tianshan (Zhu et al. 2009; Zhang et al. 2012; Wang et al. 2017, 2019) and eclogite from the Chinese South Tianshan indicate that the amalgamation among the Yili blocks and the Junggar terrane is believed to have ceased before 316 Ma (Su et al. 2010; Han et al. 2010). Late Carboniferous granitoid intrusions around 300 Ma are usually sparse and small,

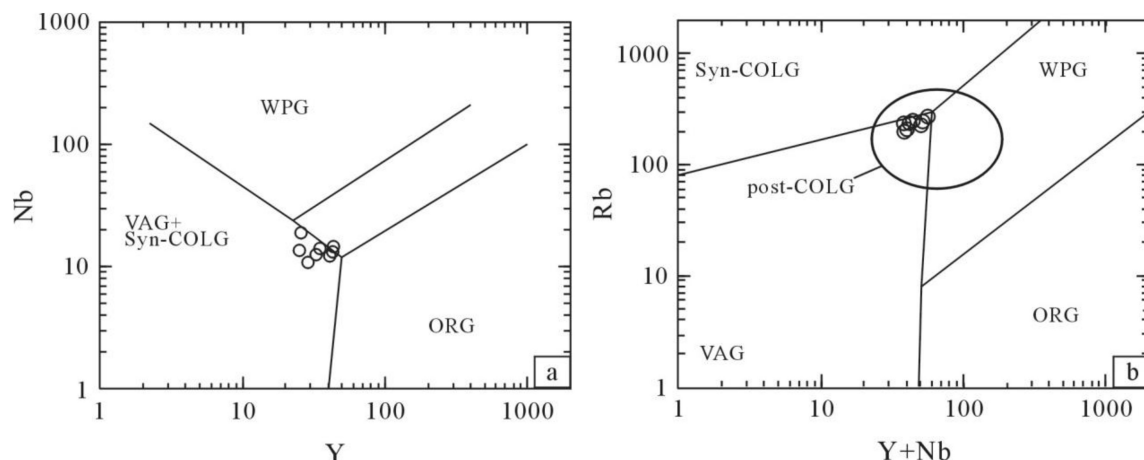


**Fig. 11** Discrimination diagrams for settings of the granites (after Pearce et al. 1984). *VAG* volcanic arc granites, *Syn-COLG* syncollisional granites, *post-COLG* post collisional granites, *ORG* ocean ridge granite, *WPG* within plate granite

such as Baideqiaoke, Zhongyangchangdaoban, Zeke-taibei, Nuoerxibei and Wulangdaban intrusions (Li 2013), which is distinctly different from widely distributed Carboniferous arc-related volcanic rocks in the Western Tianshan (Chen et al. 2013; Ma et al. 2015; Zhang et al. 2016; Zhao et al. 2018; Du et al. 2018). The intrusive rock assemblage formed in this period is gabbro diorite, granitic porphyry, granite-alkali feldspar granite. The magmatism is characterized by middle-K calc-alkaline series, high-K calc-alkaline series and potassium basaltic series, and A-type granite appears in the late stage (Li 2013). The 306.8 Ma Dunde syenogranite is high-K calc-alkaline series, and has moderate enrichment in LREE and LILEs and distinct negative Ba, Sr, Eu, P, and Ti anomalies, with mild negative Na-Ta anomalies. In the discriminant diagrams of the tectonic environment the Dunde syenogranite plot in the field of volcanic arc + syncollisional granites in the Nb-Y diagram, and in the volcanic arc granites and post-collisional granites (Fig. 11). The Yishijilike Formation in the Late Carboniferous is marked by bimodal volcanic rocks, and the Dongtujinhe formation is residual Marine clastic sedimentary in the Late Carboniferous, while the Keguqinshan formation is mainly continental coarse clastic rock. These characteristics indicate the Awulale metallogenetic belt experienced a tectonic transformation in the late Carboniferous (Li et al. 2007; Li 2013). Therefore, it is concluded that the 306.8 Ma Dunde syenogranite in the Awulale area was formed in a post-collision extensional tectonic setting.

The ore bodies of the Dunde deposit are hosted in basaltic tuff and purplish-red andesite of the Late Carboniferous Dahalajunshan Formation. Recent zircon U-Pb ages for the volcanic rocks in the deposit are in the range of 316 – 320.6 Ma (Duan et al. 2014; Jing 2016), which is

similar to the age of the volcanics in the AMB (Feng et al. 2010; Jing 2016; Zhang et al. 2012), indicating the main iron mineralization age. Different from other deposits in the AMB, the Dunde deposit contains 1,286,100 tons of zinc metals and 28.91 tons of gold (Ding 2017), and the zinc-gold mineralization mainly occurred in the hydrothermal metallogenetic stage, and the Re-Os age of pyrite associated with the zinc mineralization is  $301.2 \pm 2.4$  Ma (Kang 2018). So, the here 306.8  $\pm$  1.0 Ma granites intruded the volcanics have no alteration in the deposit, which is in accordance with the Re-Os age of pyrite associated with the zinc mineralization (Li et al. 2022), indicating that the time of the zinc-gold mineralization could be from 320 to 306.8 Ma and later than the main epoch of iron mineralization. Based on the 306.8 Ma granites are not contacted with limestone and are far from the area where ore bodies and mineralized altered rocks are widely developed, which is different from the skarn-type deposit. This epoch granites intruding the volcanics may have provided heat for the early volcanic rocks, activating the metals such as zinc and gold in the volcanic rocks to mineralization.

## 7 Conclusions

In this study, zircon U-Pb dating shows the granite from the Dunde iron-zinc polymetallic mining area was crystallized at  $306.8 \pm 1.0$  Ma. The data presented here in combination with geochronology of the volcanic rocks in the mining area could constrain the metallogenetic age from 320 to 306.8 Ma. The Dunde granites are of highly fractionated I-type granites in a post-collision extensional tectonic setting and they could be derived from the juvenile

lower crust. This epoch granites may have provided heat for the early volcanic rocks, activating the metals such as zinc and gold in the volcanic rocks to mineralization.

**Acknowledgements** This work is supported by Special Fund for Basic Scientific Research of Central Colleges, Chang'an University (Grant No.: 300102279210), the Natural Science Foundation of Shaanxi Province (Grant No.: 2019JQ-690), and the geological and mineral survey evaluation project of China Geological Survey (Grant No.: DD20190065). We are grateful to Mr. Chen Jianzhong of the Three Geological Team of the Xinjiang Bureau of Geology and Mineral Resources for the assistance in the field.

**Author contributions** ZX conceived of the presented idea. ZX and HD conduct field research. ZX, HD and YR discussed the results of the experiments and wrote the manuscript.

## Declarations

**Conflict of interest** The authors declare no conflicts of interest.

## References

- Allen MB, Windley BF, Zhang C (1992) Palaeozoic collisional tectonics and magmatism of the Chinese Tien Shan, Central Asia. *Tectonophysics* 220:89–115
- Amit M, Oded N, Ludwik H et al (2003) The petrogenesis of A-type Magmas from the Amram Massif, Southern Israel. *J Petrol* 44(5):815–832
- Barth MG, Rudnick MWF (2000) Tracking the budget of Nb and Ta in the continental crust. *Chem Geol* 165:197–213
- Blundy JD, Shimizu N (1991) Trace element evidence for plagioclase recycling in calc-alkaline magmas. *Earth Planet Sci Lett* 102:178–197
- Chappell BW, White AJR (1974) Two contrasting granite types. *Pac Geol* 8:173–174
- Che ZC, Liu L, Liu HF, Luo JH (1996) Review on the ancient Yili rift, Xinjiang, China. *Acta Petrol Sin* 12:478–490 (in Chinese with English abstract)
- Chen B, He JB, Chen CJ, Muhetaer Z (2013) Nd–Sr–Os isotopic data of the Baishiquan mafic-ultramafic complex from East Tianshan, and implications for petrogenesis. *Acta Petrol Sin* 29:294–302 (in Chinese with English abstract)
- Clarkde DB (1981) The mineralogy of peraluminous granites: a review. *Can Mineral* 19(1):3–17
- Ding HB (2017) Metallogenetic condition and origin of dunde iron-zinc deposit in western Tianshan Mountains. *Geol Rev* 64:219–220 (in Chinese)
- Du L, Long XP, Yuan C, Zhang YY, Huang ZY, Sun M, Xiao WJ (2018) Petrogenesis of Late Paleozoic diorites and A-type granites in the central Eastern Tianshan, NW China: Response to post-collisional extension triggered by slab breakoff. *Lithos* 318–319:47–59
- Duan SG, Zhang ZH, Jiang ZS, Zhao J, Zhang YP, Li FM (2014) Geology, geochemistry, and geochronology of the Dunde iron-zinc ore deposit in Western Tianshan, China. *Ore Geol Rev* 57:441–461
- Eby GN (1990) The A-type granitoids, a review of their occurrence and chemical characteristics and speculations on their petrogenesis. *Lithos* 26:115–134
- Eby GN (1992) Chemical subdivision of the A-type granitoids: petrogenetic and tectonic implications. *Geology* 20:641–644
- Ewart A, Griffin WL (1994) Application of proton-microprobe data to trace-element partitioning in volcanic rocks. *Chem Geol* 117:251–284
- Feng JX, Shi FP, Wang BY, Hu JM, Wang JT, Tian JQ (2010) The syngenetic volcanogenic iron ore deposits in Awulale Metallogenic Belt Western Tianshan Mountains. Beijing, Geological Publishing Hous, pp 1–132 (in Chinese)
- Fenn PM (1986) On the origin of graphic granite. *Am Miner* 71(3–4):325–330
- Furman TY, Bryce JG, Karson J, Iotti A (2004) East African rift system (EARS) plume structure: insight from quaternary mafic lavas of Turkana, Kenya. *J Petrol* 45:1069–1088
- Gao J, Li MS, Xiao XC, Tang YQ, He GQ (1998) Paleozoic tectonic evolution of the Tianshan Orogen, northwestern China. *Tectono-physics* 287:213–231
- Gao J, Long LL, Klemd R, Qian Q, Liu DY, Xiong XM, Yang FQ (2009) Tectonic evolution of the South Tianshan Orogen and adjacent regions, NW China, Geochemical and age constraints of granitoid rocks. *Int J Earth Sci* 98:1221–1238
- Ge SS, Du YS, Wang SX et al (2014) Genesis of skarn from Dunde iron deposit in western Tianshan, Xinjiang: mineralogical and REE constraints. *Geoscience* 28:61–72 (in Chinese with English abstract)
- Geng JZ, Qiu KF, Gou ZY, Yu HC (2017) Tectonic regime switcheroo of Triassic Western Qinling Orogen: constraints from LAICP-MS zircon U-Pb geochronology and Lu-Hf isotope of Dangchuan intrusive complex in Gansu, China. *Geochemistry* 77(4):637–651
- Gill JB (1981) Orogenic andesites and plate tectonics. Springer, Berlin, p 390
- Green TH (1995) Significance of Nb/Ta as an indicator of geochemical processes in the crust-mantle system. *Chem Geol* 120:347–359
- Gualda GAR, Ghiorso MS (2013) Low-pressure origin of high-silica rhyolites and granites. *J Geol* 121:537–545
- Han BF, Guo ZJ, Zhang ZC, Zhang L, Chen JF, Song B (2010) Age, geochemistry, and tectonic implications of a Late Paleozoic stitching pluton in the North Tian Shan suture zone, western China. *Geol Soc Am Bull* 122:627–640
- Hong W, Zhang ZH, Jiang ZS, Li FM, Liu XZ (2012) Magnetite and garnet trace element characteristics from the Chagangnuoer iron deposit in the western Tianshan Mountains, Xinjiang, NW China: Constrain for ore genesis. *Acta Petrol Sin* 28:2089–2102 (in Chinese with English abstract)
- Hu AQ, Jahn BM, Zhang GX, Chen YB, Zhang QF (2000) Crustal evolution and Phanerozoic crustal growth in northern Xinjiang, Nd isotopic evidence Part I Isotopic characterization of basement rocks. *Tectonophysics* 328:15–51
- Huang WL, Wyllie PJ (1975) Melting reactions in the system to 35 kilobars, dry and with excess water. *J Geol* 83(6):737–748
- Jackson SE, Pearson NJ, Griffin WL, Belousova EA (2004) The application of laser ablation-inductively coupled plasma-mass spectrometry to in situ U-Pb zircon geochronology. *Chem Geol* 211:47–69
- Jiang ZS, Zhang ZH, Wang ZH, Duan SG, Li FM, Tian JQ (2014) Geology, geochemistry, and geochronology of the Zhibo iron deposit in the western Tianshan, NW China: Constraints on metallogenesis and tectonic setting. *Ore Geol Rev* 57:406–424
- Jiang ZS, Zhang ZH, Wang ZH, Li FM, Tian JQ (2012) Alteration mineralogy, mineral chemistry and genesis of Zhibo iron deposit in western Tianshan Mountains, Xinjiang. *Mineral Depos* 31(5):1051–1066 (in Chinese with English abstract)
- Jing DL (2016) Mineralization and metallogenetic regularity of awulale metallogenetic belt in Western Tianshan Mountian, Northwest China. Chang'an University, A Dissertation Submitted for the Degree of Doctor, pp 1–165

- Kang YJ (2018) Ore genesis of the dunde iron-zinc-gold polymetallic deposit, West Tianshan, Xinjiang. Ph.d thesis. Peking University (in Chinese with English abstract)
- Kong H, Li H, Wu QH, Xi XS, Dick JM, Gabo-Ratio JAS (2018) Co-development of Jurassic I-type and A-type granites in southern Hunan, South China: Dual control by plate subduction and intraplate mantle upwelling. *Chem Erde* 78:500–520
- Kirkham RV, Sinclair WD (1988) Comb quartz layers in felsic intrusions and their relationship to porphyry deposits. In: Taylor RP, Strong DF (eds) Recent advances in the geology of granite related mineral deposits. The Canadian Inst Mining and Metallurgy, vol 39, pp 50–71
- Li CH, Shen P, Zhang XL, Shi FP, Feng HX, Pan DD, Wu Y, Li WG (2020) Mineralogy and mineral chemistry related to the Au mineralization in the Dunde Fe-Zn deposit, western Tianshan. *Ore Geol Rev* 124:103650
- Li HX, Zhang ZC, Liu BX, Jin YL, Santosh M, Pan JY (2022) Superimposed zinc and gold mineralization in the Dunde iron deposit, western Tianshan, NW China: constraints from LA-ICP-MS fluid inclusion microanalysis. *Ore Geol Rev* 14:10473
- Li Y (2013) Research of granite formation and tectonic environment of the Awulale region, Western Tianshan Mountain, China. Chang'an University, A Dissertation Submitted for the Degree of Master, pp 1–104
- Li X, Li Z, Wingate MTD, Chung S, Liu Y, Lin G, Li W (2006) Geochemistry of the 755 Ma Mundine Well dyke swarm, Northwestern Australia: part of a Neoproterozoic mantle superplume beneath Rodinia? *Precambr Res* 146:1–15
- Li YJ, Yang GX, Guo WJ et al (2007) The disintergration and geological significance of the Kuoerku granite batholith in Awulale, Western Tianshan Xinjiang. *Geology* 25(3):233–236 (in Chinese with English abstract)
- Li JL, Su W, Zhang X, Liu X (2009) Zircon Cameca U-Pb dating and its significance for granulite-facies gneisses from the western Awulale Mountain, West Tianshan, China. *Geol Bull China* 28:1852–1862 (in Chinese with English abstract)
- Ma XX, Shu LS, Meert JG (2015) Early Permian slab breakoff in the Chinese Tianshan belt inferred from the post-collisional granitoids. *Gondwana Res* 27:228–243
- Maniar PD, Piccoli PM (1989) Tectonic discrimination of granitoids. *Geol Soc Am Bull* 101:635–643
- Pearce JA, Harris NB, Tindle AG (1984) Trace element discrimination diagram for tectonic interpretation of granitic rocks. *J Petrol* 25:656–682
- Peccerillo A, Barberio MR, Yirgu G et al (2004) Relationships between mafic and peralkaline Silicic magmatism in continental rift setting: a petrological, geochemical and isotopic study of the Gedemsa Volcano, central Ethiopian rift. *J Petrol* 44(11):2003–2032
- Qian Q, Gao J, Klemd R, He GQ, Song B, Liu DY, Xu RH (2009) Early Paleozoic tectonic evolution of the Chinese South Tianshan Orogen: constraints from SHRIMP zircon U-Pb geochronology and geochemistry of basaltic and dioritic rocks from Xiate, NW China. *Int J Earth Sci* 98:551–569
- Su W, Gao J, Klemd R, Li JL, Zhang X, Li XH, Chen NS, Zhang L (2010) U-Pb zircon geochronology of Tianshan eclogites in NW China: implication for the collision between the Yili and Tarim blocks of the southwestern Altaiids. *Eur J Miner* 22:473–478
- Sun SS, McDonough WF (1989) Chemical and isotopic systematics of oceanic basalts: implications for mantle composition and processes. In: Saunders A, Norry M (eds) Magmatism in the Ocean Basin. Geological Society of London, pp 313–345
- Tuttle OF, Bowen NL (1958) Origin of granite in light of recent experimental studies in the system NaAlSi<sub>3</sub>O<sub>8</sub>–KAlSi<sub>3</sub>O<sub>8</sub>–SiO<sub>2</sub>–H<sub>2</sub>O. *Geol Soc Am* 74:15–62
- Vervoort JD, Blachert TJ (1999) Evolution of the depleted mantle: Hf isotope evidence from juvenile rocks through time. *Geochim Cosmochim Acta* 63:533–556
- Wang B, Shu L, Cluzel D, Faure M, Charvet J (2007) Geochemical constraints on Carboniferous volcanic rocks of the Yili Block (Xinjiang, NW China): implication for the tectonic evolution of Western Tianshan. *J Asian Earth Sci* 29:148–159
- Wang B, Faure M, Shu LS, Cluzel D, Charvet J, De Jong K, Chen Y (2008) Paleozoic tectonic evolution of the Yili Block, western Chinese Tianshan. *Bull Soc Geol Fr* 179:483–490
- Wang BY, Hu XJ, Wang JT et al (2011) Geological characteristics and genesis of Chagannur iron deposit in western Tianshan, Xinjiang. *Miner Depos* 30:385–402 (in Chinese with English abstract)
- Wang B, Liu HS, Shu LS, Jahn B, Chung SL, Zhai YZ, Liu DY (2014a) Early Neoproterozoic crustal evolution in northern Yili Block, insights from migmatite, orthogneiss and leucogranite of the Wenquan metamorphic complex in the NW Chinese Tianshan. *Precambr Res* 242:58–81
- Wang ZQ, Chen B, Ma XH (2014b) Petrogenesis of the Late Mesozoic Guposhan composite plutons from the Nanling range, South China: Implications for W-Sn mineralization. *Am J Sci* 314(1):235–277
- Wang BY, Jing DL, Jiang CY, Zhang B, Wang ZX, Shi FP (2017) Geologic background and metallogenetic mechanism of the eastern Awulale volcanic-hosted iron metallogenic belt in the western Tianshan. *Acta Petrol Sin* 33:385–397 (in Chinese with English abstract)
- Wang BY, Jing DL, Zhang B, Han L, Jiang CY (2019) Petrology and geochemistry of Carboniferous volcanic rocks from the Awulale Iron Metallogenic Belt in the West Tianshan Orogen (NW China): constraints on petrogenesis and tectonic setting. *Geol J* 54:2347–2363
- Weis D, Kieffer B, Maerschalk C, Barling, J, De Jong J, Williams GA, Hanano D, Pretorius W, Mattielli N, Scoates JS (2006) High-precision isotopic characterization of USGS reference materials by TIMS and MC-ICP-MS. *Geochemistry Geophysics Geosystems* 7:Q08006
- Whalen JB, Currie KL, Chappell BW (1987) A-type granites: geochemical characteristics, discrimination and petrogenesis. *Contrib Miner Petrol* 95:407–419
- Whalen JB, McNicoll VJ, Staal CR, Lissenberg CJ, Longstaffe FJ, Jenner GA, Breeman O (2006) Spatial, temporal and geochemical characteristics of Silurian collision-zone magmatism, Newfoundland Appalachians, an example of a rapidly evolving magmatic system related to slab break-off. *Lithos* 89:377–404
- Wu FY, Jahn BM, Wilde SA, Lo CH, Yui YF, Lin Q, Ge WC, Sun DY (2003) Highly fractionated I-type granites in NE China (I): geochronology and petrogenesis. *Lithos* 66:241–273
- Wyllie PJ, Osmaston MF, Morrison MA (1984) Constraints imposed by experimental petrology on possible and impossible magma sources and products (and Discussion). *Philos Trans Roy Soc A Math Phys Eng Sci* 310(1514):439–456
- Xia LQ, Xia ZC, Xu XY, Li XM, Ma ZP, Wang LS (2004) Carboniferous Tianshan igneous megaprovince and mantle plume. *Geol Bull China* 23:903–910 (in Chinese with English abstract)
- Xiao WJ, Zhang LC, Qin KZ, Sun S, Li JL (2004) Paleozoic accretionary and collisional tectonics of the Eastern Tianshan (China): implications for the continental growth of central Asia. *Am J Sci* 304:370–395
- Yan S, Niu HC, Zhao JX, Bao ZW, Sun WD (2018) Ore-fluid geochemistry and metallogeny of the Dunde iron-zinc deposit in western Tianshan, Xinjiang, China: evidence from fluid inclusions, REE and C–O–Sr isotopes of calcite. *Ore Geol Rev* 86:441–456

- Yan S, Zhou RJ, Niu HC, Feng YX, Nguyen AD, Zhao ZH, Yang WB, Dong Q, Zhao JX (2020) LA-MC-ICP-MS U-Pb dating of low-U garnets reveals multiple episodes of skarn formation in the volcanic-hosted iron mineralization system, Awulale belt. *Central Asia GSA Bull* 132(5–6):1031–1045
- Zen E (1986) An aluminum enrichment in silicate melts by fractional crystallization, some mineralogical and petrographic constraints. *J Petrol* 27:1095–1118
- Zhang X, Tian JQ, Gao J, Klend R, Dong LH, Fan JJ, Jiang T, Hu CJ, Qian Q (2012) Geochronology and geochemistry of granitoid rocks from the Zhibo syngenetic volcanogenic iron ore deposit in the Western Tianshan Mountains (NW-China): constraints on the age of mineralization and tectonic setting. *Gondwana Res* 22:585–596
- Zhang XR, Zhao GC, Eizenhöfer PR, Sun M, Han YG, Hou WZ, Liu DX, Wang B, Liu Q, Xu B, Zhu CY (2016) Tectonic transition from Late Carboniferous subduction to Early Permian post-collisional extension in the Eastern Tianshan, NW China: insights from geochronology and geochemistry of mafic-intermediate intrusions. *Lithos* 256–257:269–281
- Zhao RF, Chen XH, Wang QM, Liu T, Bai HH, Yuan YJ, Li CA (2006) New discoveries and prospecting potential in Western-southwestern Tianshan metallogenic. *Northwest Geol* 39(2):34–56 (in Chinese with English abstract)
- Zhao LD, Chen HY, Zhang L, Zhang WF, Yang JT, Yan XL (2018) The Late Paleozoic magmatic evolution of the Aqishan-Yamansu belt, Eastern Tianshan: constraints from geochronology, geochemistry and Sr–Nd–Pb–Hf isotopes of igneous rocks. *J Asian Earth Sci* 153:170–192
- Zhu YF, Guo X, Song B, Zhang LF, Gu LB (2009) Petrology, Sr, Nd, Hf isotopic geochemistry and zircon chronology of the Late Palaeozoic volcanic rocks in the southwestern Tianshan Mountains, Xinjiang, NW China. *J Geol Soc* 166:1085–1099

Springer Nature or its licensor (e.g. a society or other partner) holds exclusive rights to this article under a publishing agreement with the author(s) or other rightsholder(s); author self-archiving of the accepted manuscript version of this article is solely governed by the terms of such publishing agreement and applicable law.